Available online at www.sciencedirect.com

ScienceDirect

Geochimica et Cosmochimica Acta 299 (2021) 151–162

Geochimica et Cosmochimica Acta

www.elsevier.com/locate/gca

# Pedogenic processes in loess-paleosol sediments: Clues from Li isotopes of leachate in Luochuan loess

Mao-Yong He [a,b,*], Ji-Bao Dong [a,b], Zhangdong Jin [a,b,c,*], Chun-Yao Liu [d], Jun Xiao [a,b], Fei Zhang [a,b], He Sun [e], Zhi-Qi Zhao [f], Long-Fei Gou [a], Wei-Guo Liu [a,b], Chong-Guang Luo [g], You-Gui Song [a,b], Long Ma [h], Li Deng [a,b,i,j]

[a] *State Key Laboratory of Loess and Quaternary Geology, Institute of Earth Environment, Chinese Academy of Sciences, Xi'an 710061, China*
[b] *CAS Center for Excellence in Quaternary Science and Global Change, Xian 710061, China*
[c] *Institute of Global Environmental Change, Xi'an Jiaotong University, Xi'an 710049, China*
[d] *London Geochemistry and Isotope Centre (LOGIC), University College London, Gower Place, London WC1E 6BT, UK*
[e] *School of Resources and Environmental Engineering, Hefei University of Technology, Hefei 230009, China*
[f] *School of Earth Science and Resources, Chang'an University, Xi'an 710054, China*
[g] *State Key Laboratory of Ore Deposit Geochemistry, Institute of Geochemistry, Chinese Academy of Sciences, Guiyang 550002, China*
[h] *State Key Laboratory of Continental Dynamics and Shaanxi Key Laboratory of Early Life and Environment, Department of Geology, Northwest University, Xi'an 710069, China*
[i] *Shaanxi Key Laboratory of Accelerator Mass Spectrometry Technology and Application, Xi'an 710061, China*
[j] *The Chinese Loess Plateau, Critical Zone and Terrestrial Surface Flux, National Observation and Research Station, Xi'an 710061, China*

Received 1 November 2020; accepted in revised form 14 February 2021; available online xxxx

**Abstract**

Tracing pedogenic processes is fundamental for reconstructing climatic and environmental changes using loess deposits. Lithium isotopes can serve as a sensitive tracer to unravel these processes, owing to its active behaviors without effect by redox and biological reactions. This study investigated the Li contents and $\delta^7$Li values of leachate and residue ($[Li]_{leachate}$, $[Li]_{residue}$, $\delta^7Li_{leachate}$ and $\delta^7Li_{residue}$) of the upper 12.5 m Luochuan loess-paleosol sediment (since the last interglacial) on the Chinese Loess Plateau, in order to better understand pedogenic processes in loess. The $[Li]_{leachate}$, varying from 0.39 to 1.97 μg/g, is mainly derived from the adsorption phase, with a significant variation in $\delta^7Li_{leachate}$, from −6.55‰ to +12.88‰. Both $[Li]_{leachate}$ and $\delta^7Li_{leachate}$ variations reflect weathering and adsorption processes during different periods. The $[Li]_{residue}$ vary from 34.4 to 46.3 μg/g (averaging 38.4 μg/g) and their $\delta^7Li_{residue}$ vary from −3.66‰ to +2.44‰ (averaging −0.22 ± 1.68‰), both in agreement with the upper continental crust values. At initial stage after loess deposited (stage I), high $[Li]_{leachate}$ but low $\delta^7Li_{leachate}$ are results of preferential adsorption of $^6$Li by clays and migration of $^7$Li with soil solution during weathering and eluviation processes. When overlying loess was deposited and experienced pedogenesis as the stage I, $^7$Li migrated downward and was adsorbed by clays (stage II), resulting in high $[Li]_{leachate}$ and $\delta^7Li_{leachate}$ in underlying loess. When loess has superimposed pedogenic and adsorption processes as the stages I and II, loess became as paleosol with highest $\delta^7Li_{leachate}$ in underlying carbonate accumulation layer. A persistent increase in $\delta^7Li_{leachate}$ indicates dominant control of post-depositional adsorptions on Li fractionation along solution migrations during weathering and eluviation of overlying

* Corresponding authors at: State Key Laboratory of Loess and Quaternary Geology, Institute of Earth Environment, Chinese Academy of Sciences, China.
*E-mail addresses:* hemy@ieecas.cn (M.-Y. He), zhdjin@ieecas.cn (Z. Jin).

https://doi.org/10.1016/j.gca.2021.02.021

deposits, and vice versa. These results highlight that variations in $[Li]_{leachate}$ and $\delta^7Li_{leachate}$ can be used to trace soil water migration processes and the magnitude of pedogenic processes in loess-paleosol sediment at different periods.


*Keywords:* Lithium isotopic composition; Loess-paleosol deposits; Pedogenic processes; Weathering; Eluviation; Migration

## 1. INTRODUCTION

Chinese loess is one of the best terrestrial archives of late Cenozoic climatic and environmental changes and is regarded as one of the three pillars of past climate change studies. A variety of physical and geochemical proxies for weathering intensity have been explored to understand loess provenances, environmental and climatic variations in the regions of deposition (Beck et al., 2018; Sun et al., 2019). However, post-depositional pedogenic processes, including weathering and its associated secondary mineral formation, eluviation, and migration, may potentially alter mineral components and geochemical signatures of the loess-paleosol sequence (Kemp, 2001; Sun et al., 2010). As a result, most of the proxies contain mixed information on a variety of pedogenic processes, which may provide an incomplete understanding, or misinterpretations in some cases, of the paleoclimatic and paleoenvironmental conditions. Thus, a better understanding of various pedogenic processes is of priority to reconstruct paleoclimatic and paleoenvironmental changes using loess-paleosol deposits. Lithium (Li) isotope system has emerged as a potential proxy to trace pedogenic processes because of its fluid activity and not affected by redox reactions or biological processes (Rudnick et al., 2004). For example, Li isotopes in saprolites/weathering profiles have been used to understand weathering and soil-atmosphere-biosphere exchanges and to address Li isotopic behaviors (Huh et al., 2002; Rudnick et al., 2004; Teng et al., 2010; Li et al., 2020). However, the Li geochemical behaviors in loess-paleosol profiles are poorly understood so far.

Lithium (Li) has two naturally occurring isotopes, $^6Li$ (7.59%) and $^7Li$ (92.41%). The relatively large mass difference (~16%) between the two isotopes and their high volatility result in significant Li isotopic variations in natural materials (Misra and Froelich, 2012; Tomascak et al., 2016; Penniston-Dorland et al., 2017). Similar to other alkali metals, Li only has a monovalent state and is not a nutrient element. Hence, the isotopic composition of Li is not affected by redox reactions or biological processes (Rudnick et al., 2004). As an excellent tracer of fluid-rock reactions, Li isotopes in loess-paleosol may provide new insights into pedogenic processes (Tomascak et al., 2016; Teng et al., 2017). On the one hand, due to its homogeneous and continuous deposition, loess has been used to estimate the average Li composition of the upper continental crust (UCC) (Teng et al., 2004; Sauzéat et al., 2015). On the other hand, there are various Li concentrations ([Li]) in interbedded loess and paleosol, with lower $\delta^7Li$ values than primary mantle-derived igneous rocks (Tsai et al., 2014; Sauzéat et al., 2015), which is considered to be associated with weathering intensity. For example, Tsai et al. (2014) chemically separated loess samples into carbonate fractions and detritus in the Weinan profile on the southern Chinese Loess Plateau (CLP). Their results demonstrated that the $\delta^7Li$ values in carbonates were well correlated with chemical index of alteration (CIA), while the [Li] and $\delta^7Li$ in the detritus were homogeneous.

Based upon $\delta^7Li$ measurements of desert and loess deposits (windblown dust) from Europe, Argentina, China, and Tajikistan (Sauzéat et al., 2015), desert samples are thought to be more homogeneous than loess and are therefore served as a better proxy for the average Li compositions of the UCC ($[Li] = 30.5 \pm 3.6$ ppm, $\delta^7Li = 0.6 \pm 0.6‰$ (2σ)). In contrast, the $\delta^7Li$ values of loess deposits had a significant correlation with CIA, resulting from weathering processes after loess deposited (Sauzéat et al., 2015). However, little is known regarding the response of Li isotopes to pedogenic processes, and the controlling mechanisms of [Li] and $\delta^7Li$ values during weathering and pedogenesis.

The effect of post-depositional pedogenic processes of loess is relatively weak, which is mainly manifested as carbonate leaching and reprecipitation. Since adsorption and carbonate fractions are easily dissolved in acid solution, acid-leachate is representative products of pedogenic or weathering processes in loess sediments (Guo et al., 1994). In this study, we present [Li] and $\delta^7Li$ values of acid leached ($[Li]_{leachate}$ as the amount of Li leached from each gram of sediment, $\delta^7Li_{leachate}$) and residue phases ($[Li]_{residue}$ and $\delta^7Li_{residue}$) of loess and paleosol samples from the upper 12.5 m loess section in the classic Luochuan profile on the CLP. The section was deposited since the last interglacial period, i.e. from S1 to S0. The aims of this study are (1) to identify the sources of Li in the leachate from loess-paleosol sediment, (2) to constrain the factors influencing the $[Li]_{leachate}$ and $\delta^7Li_{leachate}$ during weathering, and (3) to better understand pedogenic processes after loess deposition.

## 2. GEOLOGICAL SETTING AND SAMPLING

The samples were collected from the Heimugou loess section (35°45′N, 109°25′E), which is located in Potou village, approximately 5 km from Luochuan County, Shaanxi Province, China (Fig. 1). This section can be taken as a typical loess-paleosol section in the central CLP. So far, researchers have carried out detailed studies on this section from the perspectives of stratigraphy, paleontology, pedology, and geochemistry (Chen et al., 1999; Sun et al., 2010; Wu et al., 2018). The region is in the temperate climate zone with a mean annual temperature of ~10 °C, an annual rainfall of 550–650 mm and an annual evaporation of 1600–2000 mm during 1960 and 2011 (Ma et al., 2019). The

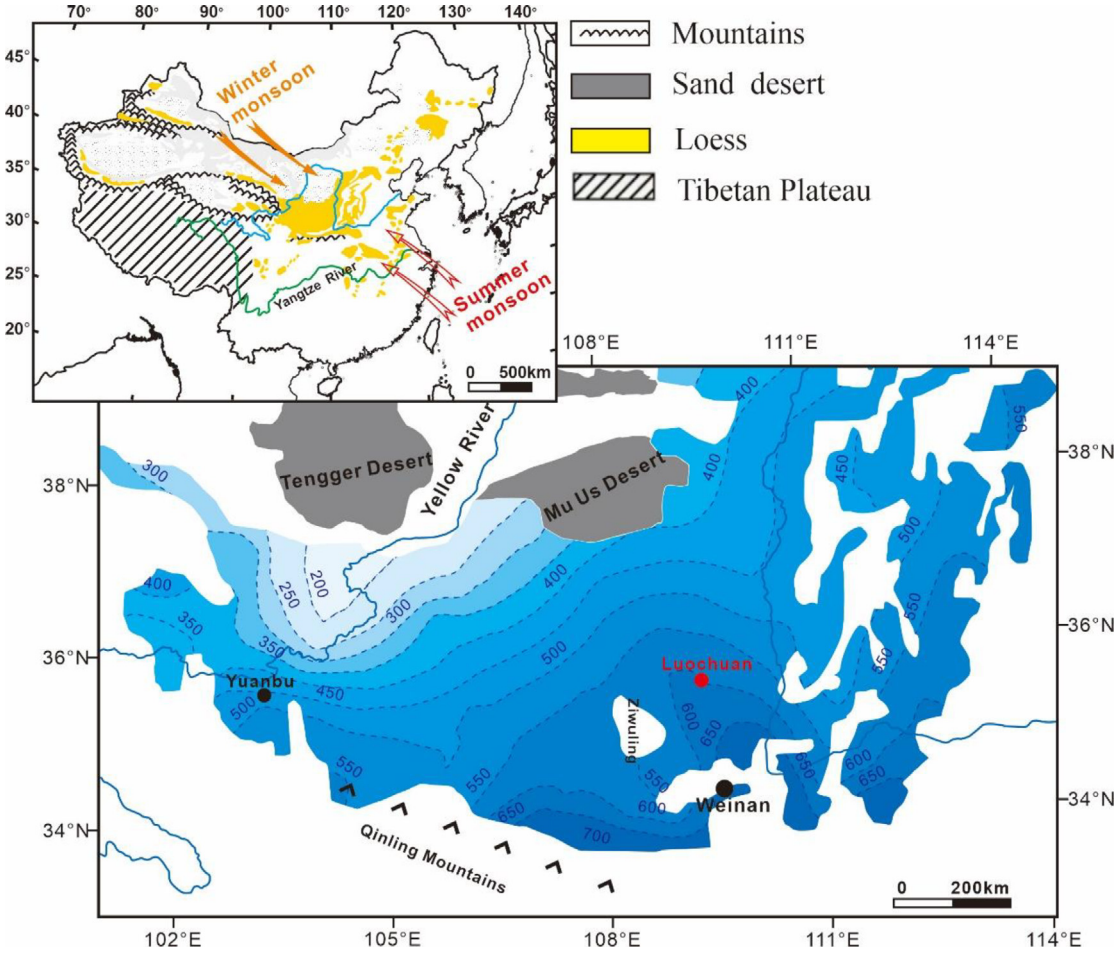


Fig. 1. Sketch map showing sampling site of Luochuan loess in this study and other loess sites mentioned in the text, including Weinan and Yuanbu. The Chinese Loess Plateau (CLP) is shadowed by contours of average annual rainfall during 1960 and 2011. The deserts and the Qinling mountains near the CLP (yellow region) are also shown. The top-left inserted China map is modified from Jin et al. (2019) showing loess distribution and the directions of the Asian summer and winter monsoons.

Luochuan Yuan (a planation surface on the CLP, loess tableland) is 1135–1160 m above sea level, with the troughs being 140 m in depth and the loess layers being approximately 130 m in thickness. To avoid any anthropogenic contamination, all of the loess and paleosol samples were systematically collected at 5 cm interval from the surface ($S_0$) stratum to 12.5 m in depth in newly excavated wells. Two carbonate nodule samples (CN1120-1 and CN1120-2) were also selected for analysis at the depth of 11.2 m, both being almost pure secondary carbonate from appearance and $CaCO_3$ content (>90%).

## 3. MATERIALS AND METHODS

### 3.1. Measurements of grain size, magnetic susceptibility, and $CaCO_3$ content

Bulk samples were analyzed for grain size, magnetic susceptibility, and $CaCO_3$ content. Prior to the measurement of grain size, all samples were pretreated by removing organic matter using 10% $H_2O_2$ and carbonates using 10% HCl, respectively (Sun et al., 2010), and were then dispersed by ultrasonication with 10 mL 10% $(NaPO_3)_6$ solution. The grain size distribution was determined using a Malvern 2000 laser instrument. Replicate analyses showed that the mean grain size had an analytical error of <2% (2 s.d.). The magnetic susceptibility was measured with a Bartington MS 2 meter. The bulk $CaCO_3$ content was measured by Elementar Soli TOC cube.

All of these measurements were carried out at State Key Laboratory of Loess and Quaternary Geology (SKLLQG), Institute of Earth Environment, Chinese Academy of Sciences (IEECAS).

### 3.2. Clay minerals analysis

The clay minerals in 18 bulk samples were extracted following the steps described by Li et al. (2018). The extracted clays were measured using an X'Pert Pro MPD powder X-ray diffractometer at the SKLLQG. Qualitative and semi-quantitative estimations of clay mineral were based on the position and intensity of peaks measured on X-ray diffraction patterns which was the same as Li et al. (2018).

### 3.3. Major elements

Prior to the measurement of major elements (Ca, Al, Na, and K), some bulk samples were pretreated by removing carbonates using 10% HCl. Then, the major elements were measured using X-ray fluorescence (XRF) spectrometer at IEECAS. The reproducibility of the elemental measurements was tested by repetitive analyses of standard loess reference sample GSS-8, and analytical uncertainties were less than 3% for all elements.

The CIA index was calculated as: $Al_2O_3/(Al_2O_3 + Na_2O + K_2O + CaO^*) \times 100$, where CaO* is the amount of CaO incorporated in the silicate fraction of the loess (Nesbitt & Young, 1982). This index was calculated using molecular proportions.

### 3.4. Lithium extraction from leachate, residue, and carbonate nodules

All bulk samples were dried at temperatures below 60 °C in an oven and were ground as fine as 200 mesh using an agate mortar, after removing the visible plant roots and other organic substances. The CN1120-1 and CN1120-2 carbonate nodule samples were also treated after removing the adhered clays.

Previous studies demonstrated that dilute acetic acid (HAc) leaching (<1 M) can dissolve all the carbonates in loess samples but does not essentially destroy the structure of detrital minerals (quartz, feldspar, clay minerals, and dolomite) (e.g. Yang et al., 2001; Wei et al., 2015). Here, the following chemical procedure using 1 M HAc was employed to leach carbonates from bulk loess and carbonate nodule samples.

(i) ~2 g of bulk sample or carbonate nodules were weighed;
(ii) Exactly 25.0 mL of 1 M HAc was added and then ultrasonically shaken for 48 h at room-temperature;
(iii) Each sample was centrifuged at 4000 rpm for 20 min to separate the residue from the leachate, and the residue was treated six times as the Step (ii);
(iv) The leachate solution collected from all cycles of the extraction was mixed and used for the ion-exchange column in the next step.

The 13 residue samples after the leaching procedure were rinsed three times using UHQ deionized water to remove remaining acid. The dried residue was weighed again and dissolved using the HF-$HNO_3$ dissolution technique described by Huang et al. (2019).

### 3.5. Chemical purification procedure of Li

Prior to the measurements of isotopic ratios, Li was separated from the sample matrix using AG50W-X8 resin (100–200 mesh; Bio-Rad, Hercules, CA, USA) packed into customized PFA microcolumns with an internal diameter of 6.4 mm and a column length of 25 cm. The resin volume used was 8.0 mL. The Li separation procedure in this study was followed previous established method using one-step ion chromatography (He et al., 2019). The HAc leachate, which contained approximately 0.2 μg Li, was dried in PFA vials at 95 °C and then dissolved in 0.5 mL 0.5 M $HNO_3$ before being loaded onto columns (0.64 × 25 cm) containing a pre-conditioned resin. The final Li solution was dried and dissolved in 2% $HNO_3$ to yield a concentration of 100 μg/L of Li for analysis. For each sample, intensities (counts/second) of $^7Li$ and $^{23}Na$ were determined by ICP-MS to check for Li column recovery, blanks, and Na/Li (by weight) ratio in the aliquots for ion-exchange-column separate and collected before and after it. This procedure ensures (1) that the collected fraction contains >99% of the total sample Li to prevent fractionation within the column and (2) that the matrix elements were limited to <3% of the concentration of Li to prevent matrix effects. The total procedural blank was less than 0.16 ng Li in this study, which is insignificant relative to the total of Li analyzed (Gou et al., 2019). The Na/Li in all of the samples reported in this study was less than 1, which has insignificant effect on the $\delta^7Li$ measurements.

### 3.6. Measurements of major and trace elements in leachate and residue

The contents of major elements (Ca, K, Mg, Na, Fe and Al) of leachate and residue samples were determined three times on iCAP™ 7400 ICP-OES (Thermo Fisher Scientific, Bremen, Germany) at the SKLLQG.

The contents of trace elements (Li and Sr) of leachate and residue samples were measured three times using a PE NexION 300D ICP-MS.

To evaluate the long-term reproducibility of precision and accuracy of major and trace elements determinations, repeat measurements of the reference materials GBW-Li, basalt (BHVO-2), andesite (AGV-2) and seawater (NASS-6) were carried out. The analytical precision (RSD) <3% was achieved for major and trace elements determinations.

### 3.7. Measurements of Li isotope ratios

All Li isotope measurements were conducted on a NEPTUNE Plus MC-ICP-MS at the SKLLQG, which enabled a static measurement of m/z 6 and m/z 7 on the low-mass Faraday cup (L4) and the high-mass Faraday cup (H4), using the sample standard bracketing (SSB) method with focus and dispersion. All samples and standards (L-SVEC) were run at a similar Li concentration.

The total procedural Li blank (including chemistry and analyses) was determined and was systematically lower than 0.16 ng, with a mean value of $0.10 \pm 0.03$ ng ($n = 10$). The external precision (2 s.d.) of the $\delta^7Li$ values was better than 0.25‰.

Three common reference materials were used to determine the precision and accuracy of the methods in this study, i.e. basalt (BHVO-2), andesite (AGV-2) and seawater (NASS-6) standards. The $\delta^7Li$ values for NASS-6, AGV-2, and BHVO-2 were $30.78 \pm 0.32$‰, $6.32 \pm 0.38$‰, and $4.23 \pm 0.35$‰, respectively, all in excellent agreement with previous studies (Table 1).

Table 1
Measured $\delta^7$Li in certified seawater and rock and comparison with reported previously.

| Samples | $\delta^7$Li (mean ± 2 s.d. ‰) | | |
|---|---|---|---|
| | This study (n = 5) | Reported | References |
| Seawater (Atlantic NASS-6) | 30.78 ± 0.32 | 30.87 ± 0.15 | Lin et al., 2016 |
| | | 31.1 ± 0.7 | Gou et al., 2019 |
| | | 30.8 ± 0.4 | Rosner et al., 2007 |
| | | 31.0 ± 0.4 | Ma et al., 2020 |
| | | 31.14 ± 0.2 | Kasemann et al., 2005 |
| | | 30.81 ± 0.38 | He et al., 2019 |
| Andesite (AGV-2) | 6.32 ± 0.38 | 6.85 ± 0.20 | Lin et al., 2016 |
| | | 6.01 ± 0.10 | He et al., 2019 |
| | | 5.68 ± 1.04 | Tian et al., 2012 |
| Basalt (BHVO-2) | 4.23 ± 0.35 | 3.9 ± 0.9 | Gou et al., 2019 |
| | | 4.46 ± 0.37 | Rosner et al., 2007 |
| | | 4.7 ± 0.6 | Li and Liu, 2020 |
| | | 4.74 ± 1.1 | Li et al., 2020 |

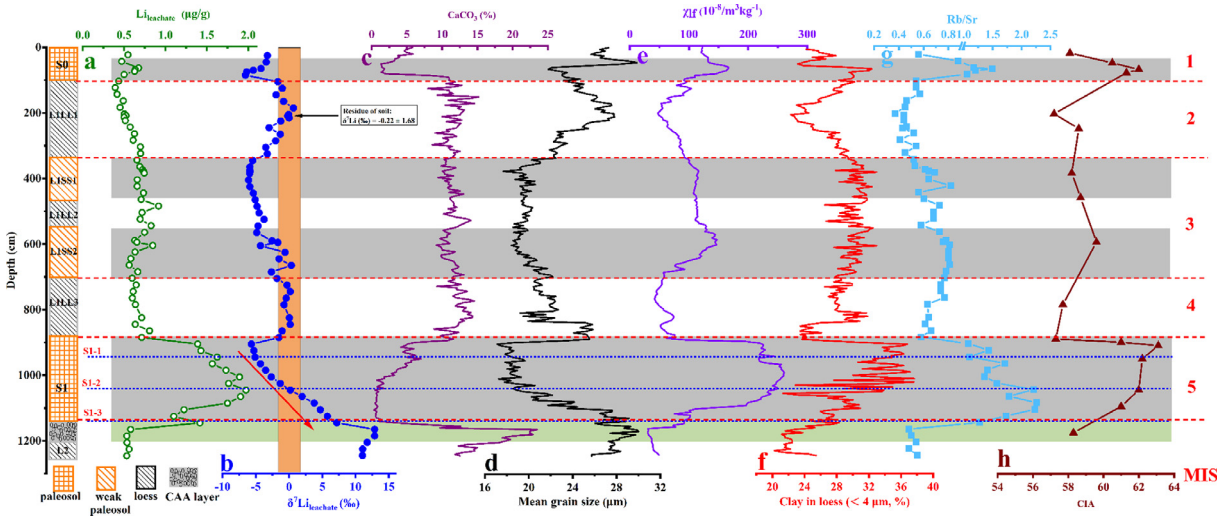


Fig. 2. Stratigraphy and variations in (a) $[Li]_{leachate}$, (b) $\delta^7Li_{leachate}$, (c) bulk $CaCO_3$ content, (d) mean grain size, (e) magnetic susceptibility, (f) clay in loess, (g) Rb/Sr ratio, and (h) CIA of the Luochuan loess since the last interglacial (S1). Paleosol and weak paleosol layers with lower $\delta^7Li_{leachate}$ indicate stronger pedogenic processes (grey shadows). The highest $\delta^7Li_{leachate}$ is found in the calcium carbonate accumulation layer (CAA, light green shadow). The red arrows show gradual increase in $\delta^7Li_{leachate}$, resulting from progressive absorption of $^6$Li by clays. The loess and paleosol layers are corresponded to the marine isotope stages (MIS) on right of the panel, labelled from 1 to 5.

## 4. RESULTS

### 4.1. Stratigraphy

The Luochuan section is typically composed of loess and paleosol layers, which can be easily identified by soil color. The stratigraphy in the present study is the same as that reported by Sun et al. (2010) and can be divided into loess and paleosol deposits, respectively, as shown in Fig. 2 and Table S1. In general, the magnetic susceptibility values tend to be higher in paleosols (S0, L1SS1, L1SS2, and S1) than those in adjacent loess deposits (L1LL1, L1LL2, L1LL3, and L2). The clay contents in paleosol layers were also higher than those in loess layers. Illite is the dominant clay mineral in the Luochuan section (averaging 70%), following by chlorite and kaolinite, with average contents of 18% and 8% in clays, respectively. The loess was deposited during glacial periods and the paleosol was formed during interglacial periods (Sun et al., 2010; Jin et al., 2019; Guo et al., 2021). The upper 12.5 m section contains a complete sequence of loess-paleosol deposits since the last interglacial, i.e., brownish paleosol S1 (11.45–8.85 m; corresponding to marine isotope stage 5 (MIS 5)), the last glacial yellowish typical loess L1 (8.85–1.05 m; MISs 4, 3, and 2), and the Holocene brownish paleosol S0 (uppermost 1.05 m, MIS 1), as shown in Fig. 2. The S1 unit includes three warm periods (MIS 5a, c, and e) and two relatively cold periods (MIS 5b and d). Owing to relatively low dust accumulation rate and strong weathering, the three paleosols of the Luochuan S1 layer are completely welded in an accretionary Mollisol-like pedocomplex (Feng and Wang, 2006). According to the carbonate content, magnetic

Table 2
[Li] and Li isotopic compositions of leachate and residue in Luochuan loess profile.

| Sample No. | Depth | [Li] (μg/g) | [Li] (μg/g) | $\delta^7$Li ± 2 s.d. (‰) | |
|---|---|---|---|---|---|
| | (cm) | leachate | residue | leachate | residue |
| LC-25 | 25 | 0.55 | 36.89 | −3.24 ± 0.08 | 1.14 ± 0.07 |
| LC-45 | 45 | 0.47 | | −3.43 ± 0.49 | |
| LC-65 | 65 | 0.68 | | −4.21 ± 0.11 | |
| LC-70 | 70 | 0.64 | | −5.36 ± 0.03 | |
| LC-75 | 75 | 0.63 | | −6.37 ± 0.04 | |
| LC-75-R | 75 | 0.62 | | −6.36 ± 0.08 | |
| LC-85 | 85 | 0.50 | | −6.55 ± 0.11 | |
| LC-105 | 105 | 0.43 | | −1.67 ± 0.08 | |
| LC-125 | 125 | 0.39 | 36.90 | −1.01 ± 0.09 | 0.25 ± 0.16 |
| LC-145 | 145 | 0.42 | | −1.94 ± 0.41 | |
| LC-165 | 165 | 0.49 | | −0.82 ± 0.07 | |
| LC-185 | 185 | 0.45 | | 0.66 ± 0.24 | |
| LC-205 | 205 | 0.50 | | −0.04 ± 0.33 | |
| LC-210 | 210 | 0.52 | | −0.20 ± 0.17 | |
| LC-215 | 215 | 0.50 | | 0.02 ± 0.03 | |
| LC-225 | 225 | 0.52 | 45.26 | −1.26 ± 0.18 | −1.20 ± 0.36 |
| LC-245 | 245 | 0.57 | | −2.98 ± 0.16 | |
| LC-265 | 265 | 0.63 | | −1.31 ± 0.13 | |
| LC-285 | 285 | 0.61 | | −2.00 ± 0.10 | |
| LC-305 | 305 | 0.70 | | −3.50 ± 0.11 | |
| LC-325 | 325 | 0.70 | | −3.26 ± 0.04 | |
| LC-325-R | 325 | 0.70 | | −3.24 ± 0.03 | |
| LC-345 | 345 | 0.66 | 35.90 | −5.45 ± 0.08 | −1.01 ± 0.36 |
| LC-365 | 365 | 0.69 | | −5.88 ± 0.49 | |
| LC-375 | 375 | 0.72 | | −5.88 ± 0.43 | |
| LC-380 | 380 | 0.74 | | −5.87 ± 0.01 | |
| LC-385 | 385 | 0.74 | | −5.91 ± 0.14 | |
| LC-405 | 405 | 0.66 | | −6.08 ± 0.03 | |
| LC-425 | 425 | 0.66 | | −5.88 ± 0.05 | |
| LC-445 | 445 | 0.74 | | −5.36 ± 0.03 | |
| LC-465 | 465 | 0.71 | | −5.08 ± 0.02 | |
| LC-485 | 485 | 0.92 | 38.05 | −4.80 ± 0.03 | −3.66 ± 0.33 |
| LC-505 | 505 | 0.72 | | −4.50 ± 0.47 | |
| LC-525 | 525 | 0.69 | | −3.76 ± 0.08 | |
| LC-545 | 545 | 0.83 | | −4.66 ± 0.10 | |
| LC-565 | 565 | 0.75 | | −4.85 ± 0.18 | |
| LC-590 | 590 | 0.63 | | −2.57 ± 0.14 | |
| LC-595 | 595 | 0.66 | 35.45 | −1.68 ± 0.14 | −0.89 ± 0.26 |
| LC-605 | 605 | 0.85 | | −4.28 ± 0.08 | |
| LC-605-R | 605 | 0.86 | | −4.27 ± 0.03 | |
| LC-625 | 625 | 0.63 | | −0.60 ± 0.14 | |
| LC-645 | 645 | 0.58 | | −1.50 ± 0.13 | |
| LC-665 | 665 | 0.56 | | 0.35 ± 0.13 | |
| LC-685 | 685 | 0.67 | 38.49 | −2.64 ± 0.04 | −0.21 ± 0.11 |
| LC-705 | 705 | 0.60 | | −1.81 ± 0.48 | |
| LC-725 | 725 | 0.65 | | −0.30 ± 0.15 | |
| LC-745 | 745 | 0.61 | 34.90 | 0.20 ± 0.02 | −2.33 ± 0.24 |
| LC-765 | 765 | 0.60 | | −0.42 ± 0.04 | |
| LC-785 | 785 | 0.64 | | −0.76 ± 0.10 | |
| LC-825 | 825 | 0.71 | | 0.06 ± 0.03 | |
| LC-845 | 845 | 0.64 | 35.83 | 0.18 ± 0.01 | −0.01 ± 0.07 |
| LC-865 | 865 | 0.81 | | −1.02 ± 0.03 | |
| LC-885 | 885 | 0.71 | | −1.52 ± 0.07 | |
| LC-905 | 905 | 1.39 | | −5.65 ± 0.08 | |
| LC-925 | 925 | 1.43 | | −5.28 ± 0.10 | |
| LC-945 | 945 | 1.62 | 46.30 | −5.10 ± 0.03 | −0.52 ± 0.17 |
| LC-965 | 965 | 1.57 | | −4.29 ± 0.07 | |
| LC-985 | 985 | 1.73 | | −3.52 ± 0.06 | |
| LC-1005 | 1005 | 1.89 | | −2.65 ± 0.07 | |
| LC-1025 | 1025 | 1.76 | | −1.32 ± 0.05 | |

| | | | | | |
|---|---|---|---|---|---|
| LC-1025-R | 1025 | 1.77 | | −1.32 ± 0.08 | |
| LC-1035 | 1035 | 1.76 | | −1.32 ± 0.05 | |
| LC-1045 | 1045 | 1.97 | 44.87 | 0.19 ± 0.43 | 1.51 ± 0.02 |
| LC-1065 | 1065 | 1.91 | | 1.97 ± 0.06 | |
| LC-1085 | 1085 | 1.75 | | 3.78 ± 0.048 | |
| LC-1105 | 1105 | 1.22 | | 4.71 ± 0.36 | |
| LC-1125 | 1125 | 1.10 | | 5.78 ± 0.43 | |
| LC-1145 | 1145 | 1.42 | 35.39 | 7.73 ± 0.12 | 2.44 ± 0.13 |
| LC-1165 | 1165 | 0.58 | | 12.88 ± 0.20 | |
| LC-1185 | 1185 | 0.53 | | 12.88 ± 0.10 | |
| LC-1185-R | 1185 | 0.52 | | 12.86 ± 0.04 | |
| LC-1205 | 1205 | 0.54 | | 11.76 ± 0.10 | |
| LC-1225 | 1225 | 0.56 | | 11.09 ± 0.11 | |
| LC-1245 | 1245 | 0.53 | 34.40 | 11.05 ± 0.11 | 1.58 ± 0.10 |

susceptibility and mean grain size, the Luochuan S1 paleosol layer can only be divided into three layers S1-1, S1-2 and S1-3 based on the method proposed by Guo et al. (1994) (Fig. 2).

### 4.2. Lithium concentrations of leachate in loess-paleosol sequence

Among the samples collected from the top 12.50 m of the Luochuan profile, the $[Li]_{leachate}$ values vary from 0.39 to 1.97 μg/g (Fig. 2; Table 2), with an average value of 0.80 μg/g; the $[Li]_{residue}$ vary from 34.40 to 46.30 μg/g with an average of 38.36 μg/g. Therefore, the $[Li]_{leachate}$ is much lower compared to the $[Li]_{residue}$. The $[Li]_{leachate}$ are relatively low in the loess layer, with values from 0.39 to 0.91 μg/g. In comparison, the $[Li]_{leachate}$ values vary from 1.01 to 1.97 μg/g in the S1 paleosol. Hence, the $[Li]_{leachate}$ values in the S1 paleosol are much higher than those in loess, which have experienced a higher degree of weathering than loess, as shown by high magnetic susceptibility and finer grain size (Fig. 2; Table 2).

### 4.3. Lithium isotopic compositions of leachate, residue, and carbonate nodules

The $\delta^7Li_{leachate}$ are ranged from −6.55‰ to +12.88‰ (Fig. 2; Table 2). Interestingly, the $\delta^7Li_{leachate}$ slowly increase to higher values and reach a maximum value of +12.88‰ from the S1 paleosol to calcium carbonate accumulation (CCA). The $\delta^7Li_{leachate}$ of two carbonate nodules (CN1120-1 and CN1120-2) are +7.24‰ and +8.49‰, with $[Li]_{leachate}$ being 10.50 ng/g and 10.40 ng/g, respectively. These nodules are almost pure secondary carbonates, with $CaCO_3$ content >90%.

The $\delta^7Li_{residue}$ vary from −3.66‰ to +2.44‰ with an average $\delta^7Li_{residue} = -0.22 \pm 1.68$‰, in agreement with the UCC values reported by Sauzéat et al. (2015).

## 5. DISCUSSIONS

### 5.1. The sources of Li in the leachate

There are three potential sources for the Li in the leachate fractions of both loess and paleosol: (1) leaching from silicate minerals (structural cation), (2) dissolving of carbonate minerals, and (3) adsorbed by clay minerals (exchangeable Li).

#### *5.1.1. Minor Li from silicate dissolution (structural cation)*

A series of leaching procedures by different acids (e.g. hydrochloric acid (HCl) and HAc) have been carried out for leachate fraction of loess (e.g. Yang et al., 2001; Wei et al., 2015). It was demonstrated that leaching detrital minerals (quartz, feldspar, clay minerals, and dolomite) have an insignificant contribution to leached Li by HAc (Lin et al., 2019; Taylor et al., 2019). Here, we employed the concentrations of Al, K, Fe and Na in the leachate fractions and bulk samples to evaluate whether 1 M HAc dissolves the silicate components or not, because these elements are not susceptible to acid dissolution in loess and paleosol. The leaching rate was calculated as the concentrations of these elements in the leachate fraction relative to bulk samples (Table S2). The results show that the leaching rates of all of these elements are much lower than 1%, indicating rather limited dissolved Li contribution of silicate minerals to the leachate fraction.

#### *5.1.2. Limited proportion of Li from the carbonate fraction of loess and paleosol*

Loess exists a large amount of detrital and secondary carbonate minerals, which may contribute Li in leachate fraction, because carbonates are easily dissolved by weak HAc. The average carbonate content of loess in the central CLP is 11.5% (Wei et al., 2015). However, Li from carbonates is not a major player for the $[Li]_{leachate}$ variation in loess-paleosol, since the $[Li]_{leachate}$ do not increase with bulk $CaCO_3$ contents as shown in Fig. 3. In fact, the $[Li]_{leachate}$ in the carbonate-rich loess and the CAA layers are even lower than those in the paleosol layer (Figs. 2 and 3). The lower Li/Ca ratios in the leachate fractions of loess and CAA layer with high carbonates was much lower than those in paleosol with lower carbonates (Table S2), further supporting limited contribution of Li in carbonate to the $[Li]_{leachate}$. Based on the averages of [Li] and $\delta^7Li$ of pure carbonate nodule samples (CN1120-1 and CN1120-2), Li from carbonates only accounts for less than 10% of the average $[Li]_{leachate}$ and <0.2% for the $\delta^7Li_{leachate}$ (Table S3). These lines of evidence indicate that the carbonate phase would account for limited proportion of Li budget in leachate fraction of both loess and paleosol.

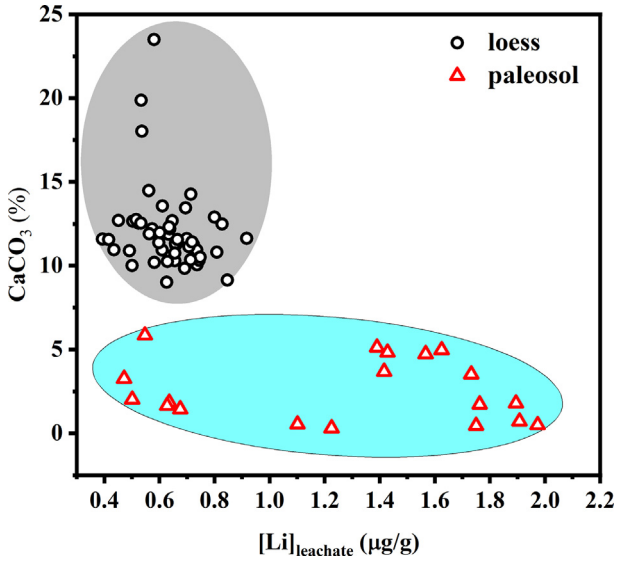


Fig. 3. The correlation between $[Li]_{leachate}$ and $CaCO_3$ content of the Luochuan loess.

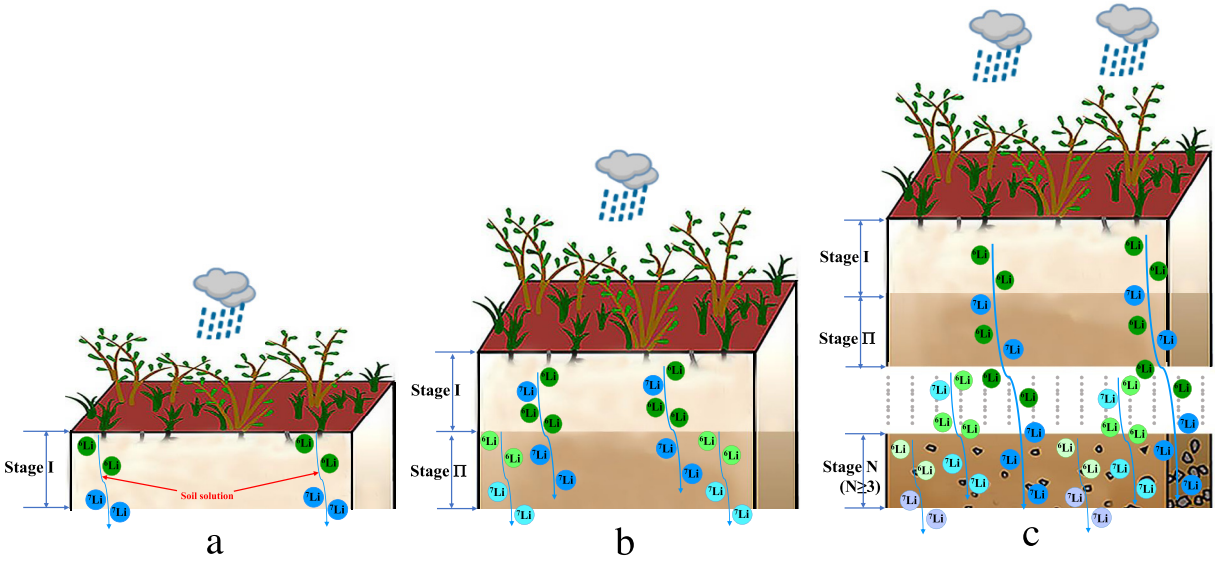


Fig. 4. A cartoon illustrating our proposed dynamical mechanism driving $\delta^7Li_{leachate}$ variability in loess profile. Stage I: Loess experienced initial weathering and eluviation after it deposited, leading to low $\delta^7Li_{leachate}$ resulting from $^7Li$ migration with soil solution; Stage II: When overlying loess deposited and experienced pedogenesis as the stage I, $^7Li$ migrated downward and adsorbed by clays in underlying loess; Stage N ($N \geq 3$): When loess has superimposed pedogenic and adsorption processes as the stages I and II, loess became as paleosols with highest $\delta^7Li_{leachate}$ in underlying carbonate accumulation layer.

*5.1.3. Li in the leachate dominated by adsorption fraction*

As observed above, dissolution of silicate and carbonate minerals is not the major sources of Li in the leachate of loess and paleosol, so that Li in the leachate of both loess and paleosol would be dominated by exchangeable Li adsorbed by clay minerals. Indeed, Li is easily adsorbed by clays and oxides and can replace $Mg^{2+}$, $Al^{3+}$, and $Fe^{2+}$ due to its high affinity (Misra and Froelich, 2012; Li and West, 2014). Because the clay contents in paleosol layers are higher than those in loess layers (Sun et al., 2010), which probably explains the higher $[Li]_{leachate}$ in paleosol than loess layers (Fig. 2). Therefore, Li adsorbed by clay minerals (exchangeable Li) is the dominated source of Li in the leachate fraction of loess-paleosol sediments.

### 5.2. Factors controlling variations of $[Li]_{leachate}$ and $\delta^7Li_{leachate}$

Loess-paleosol is eolian dust deposit which originates from finely textured materials and is transported by wind

from northern China and central Asian deserts and then is deposited on the CLP. Thus, the chemical compositional variation of loess-paleosol deposits is mainly affected by two factors: (i) provenances and (ii) pedogenic processes after deposit (Jia et al., 2007; Ma et al., 2019).

Large-scale, long-distance transport and mixing make the loess-paleosol material highly uniform. Homogeneity of Nd, Sr and Pb isotopic compositions strongly supports a uniform source for loess and paleosol, in particular since the S1 (Gallet et al., 1996). Therefore, variations of $[Li]_{leachate}$ and $\delta^7Li_{leachate}$ in loess-paleosol sequence would be mainly controlled by post-depositional pedogenic processes. Correspondingly, variable $[Li]_{leachate}$ and $\delta^7Li_{leachate}$ can be used to trace pedogenic processes after dust deposition.

Li in loess-paleosol sediment is contained in Mg-bearing and ferromagnesian minerals, mica, biotite, and tourmaline (Jia et al., 2007). During the leaching and pedogenic processes after loess deposition, part of Li can be released from the mineral lattice when silicate minerals decomposed (Jia et al., 2007). $Li^+$ in solution would migrate with soil water as the form of soluble salts (such as LiCl). Along with the migration, $Li^+$ is easily adsorbed by clay minerals, in particular in paleosol layers with high clays. As a result, the S1 layer has high $[Li]_{leachate}$ (Fig. 2). Meanwhile, the weakly developed paleosols, such as S0, L1SS1, and L1SS2 within the loess units which can be distinguished by magnetic susceptibility, also have relatively high $[Li]_{leachate}$. By contrast, the $[Li]_{leachate}$ in the loess layers are lower than those in the paleosol.

For the upper 12.5 m Luochuan loess-paleosol sediments, the values of the $\delta^7Li_{leachate}$ in loess layers are similar to the $\delta^7Li_{residue}$ (averaging $-0.22 \pm 1.68$‰), but the paleosol layers tend to have lower $\delta^7Li_{leachate}$ than $\delta^7Li_{residue}$ values (Fig. 2). However, the $\delta^7Li_{leachate}$ slowly increase from the S1-1 paleosol and reach to a maximum value of +12.88‰t at the CCA layer (Fig. 2). This observation could be explained by two potential processes: decomposition of the primary rocks and adsorption by the clay minerals. Previous studies suggest that Li isotopes do not fractionate during the decomposition of weathered and leached protoliths (Wimpenny et al., 2015; Verney-Carron et al., 2011; Liu et al., 2015), which is consistent with near uniform $\delta^7Li_{residue}$ in the loess sediments. Li isotopic fractionation mainly occurs during solution transport: the solution carries away heavier isotope ($^7Li$), resulting from $^6Li$ preferentially adsorbed by weathered products of silicates at low-temperature, dominated by clay minerals (Rudnick et al., 2004; Vigier et al., 2008; Liu and Rudnick, 2011). Therefore, the variation in the $\delta^7Li_{leachate}$ of the paleosol would be caused by adsorption onto clay minerals during pedogenic processes.

The proportion of clays and their adsorption ability are main factors controlling the $\delta^7Li_{leachate}$ values in loess-paleosol sequence, since different clays have different adsorption capacity for $Li^+$ (Misra and Froelich, 2012; Bohlin and Bickle, 2019; Li and Liu, 2020; Pogge von Strandmann et al., 2020). In the previous adsorption experiments, Li isotopic fractionations were different from clay minerals, i.e. close to 0‰ for smectite and illite, 1–3‰ for ferrihydrite and chlorite, ~7‰ for kaolinite, and >10‰ for gibbsite (Pistiner and Henderson, 2003; Millot and Girard, 2007). Increasing experiments and theoretical calculations have confirmed the kinetic controls on Li isotope fractionations (Hofmann et al., 2012; Hindshaw et al., 2019; Li and Liu, 2020). Here, we propose that repeated adsorption processes control the $\delta^7Li_{leachate}$ in loess-paleosol sequence at different stages, as a conceptual Rayleigh distillation model following a kinetic law as illustrated in Fig. 4.

At the first stage, when loess experiences initial weathering and eluviation after deposition, Li is released due to decomposition of primary minerals. Along with the downward migration of soil solution, $^6Li$ is preferentially adsorbed by clay minerals and $^7Li$ is lost to the solution (stage I, Fig. 4a). As a result, the leachate $Li^+$ in loess layers have low $\delta^7Li_{leachate}$, while soil solution with more $^7Li$ moves downwards in the profile.

When another loess layer is deposited and experiences pedogenesis as the same stage I, downward migrated $^7Li$ is adsorbed by clays in underlying loess and/or paleosol (stage II, Fig. 4b). If the loess-paleosol sequence experiences repeated pedogenic and adsorption processes as the stages I and II, more $^7Li$ would migrate downward and be adsorbed by clays in underlying paleosol. The $\delta^7Li_{leachate}$ trends to more positive when these processes continue (Fig. 4b, c). As a result, the highest $\delta^7Li_{leachate}$ appears in the CCA layer at the bottom of the underlying paleosol (stage N ($N \geq 3$), Fig. 4c). Similarly, Tsai et al. (2014) also reported highest $\delta^7Li$ (10.2‰) at the CCA layer in the S1 of the Weinan section, located at the southeastern margin of the CLP (Fig. 1). Therefore, the $\delta^7Li_{leachate}$ of the lower paleosol and the CCA layers is a result of multiple cycles of pedogenic and adsorption processes (Fig. 4b, c). The $\delta^7Li_{leachate}$ variation of loess sediments reflects the change in the magnitude or proportion of the contribution of these processes (Figs. 2 and 4). In addition, we notice higher $\delta^7Li_{leachate}$ but lower $[Li]_{leachate}$ of the L2 layer just below the S1 layer than those of the S1 layer (Fig. 2), which may attribute to horizontal groundwater flow near the S1 and L2 layers, rather than downward migration of soil solution. Further tracing for potential impact of groundwater on Li behaviors is deserved.

The $\delta^7Li_{leachate}$ of loess-paleosol sequence can be described by the following mass balance:

$$[Li]_{leachate} * \delta^7Li_{leachate} = [Li]_{ad\ stage\ I} * \delta^7Li_{ad\ stage\ I} + [Li]_{ad\ stageII} * \delta^7Li_{ad\ stage\ II} + \sum [Li]_{ad\ stage\ N} * \delta^7Li_{ad\ stage\ N} \quad (1)$$

$$[Li]_{leachate} = [Li]_{ad\ stage\ I} + [Li]_{ad\ stage\ II} + \sum [Li]_{ad\ stage\ N} \quad (2)$$

where $[Li]_{ad\ stage\ I}$, $[Li]_{ad\ stage\ II}$, and $[Li]_{ad\ stage\ N}$ are the Li content of adsorbed by clay minerals at adsorption stages I, II, …N ($N \geq 3$); correspondingly, $\delta^7Li_{ad\ stage\ I}$, $\delta^7Li_{ad\ stage\ II}$, and $\delta^7Li_{ad\ stage\ N}$ are the Li isotopic composition of adsorbed Li by clay minerals at the adsorption stage I, II, …N.

The measured $\delta^7Li_{leachate}$ in loess-paleosol sediments is controlled by mixed processes repeatedly at different stages.

However, adsorbed Li isotopes are different during these stages. At the initial pedogenic processes as the stage I, the Li isotope adsorbed by the clay minerals is mainly derived from weathered detrital minerals with low $\delta^7Li$ and the downward migrating soil solution is enriched in $^7Li$. At the subsequent stages II,...N, the Li isotope adsorbed by clay minerals mainly comes from the overlying soil solution, resulting in more $^7Li$ than that adsorbed during initial weathering and eluviation processes. The fractionation of Li isotopic compositions between soil solution and adsorbed by clay minerals during post-depositional period can be described by the following equilibria:

$$\Delta^7Li_{ad-solution} = \delta^7Li_{solution} - \delta^7Li_{ad\ stage\ II,.....N} \quad (3)$$

where $\delta^7Li_{ad\ stage\ II,\ ...N}$ is the Li isotopic composition adsorbed by clay minerals at adsorption stages II,...N; $\delta^7Li_{solution}$ is the Li isotopic composition of original soil solution. In the case of relatively stable sedimentation environment as loess, the isotope fractionation factor is unchanged, i.e., a constant $\Delta^7Li_{ad\ -\ solution}$. Under this situation, $\delta^7Li_{ad\ stage\ II,\ ...N}$ is determined by $\delta^7Li_{solution}$ only. It means that $\delta^7Li_{leachate}$ will be high when the $\delta^7Li_{solution}$ is high (Decarreau et al., 2012; Wimpenny et al., 2015; Hindshaw et al., 2019).

### 5.3. Using $\delta^7Li_{leachate}$ to trace pedogenic processes in loess sediments

During the processes of paleosol formation in loess-paleosol sequences, the elements undergo loss or gain by different degrees along with post-depositional pedogenic processes, including weathering and its associated secondary mineral formation, eluviation, and migration (Kemp, 2001; Sun et al., 2010). However, these post-depositional pedogenic processes are poorly understood so far. Here, as a sensitive tracer, the $\delta^7Li_{leachate}$ provides new insight into pedogenic processes in loess-paleosol sequences.

Firstly, when $\delta^7Li_{leachate}$ in sediments are close to the $\delta^7Li_{residue}$, it means that they are loess layers that have very weak or limited pedogenic processes of weathering and eluviation, such as L1LL1 and L1LL3 (Fig. 2). These sediments were deposited during dry and wet glacial conditions (Sun et al., 2010), characterized by high and constant $CaCO_3$ contents but low magnetic susceptibility. As a result, these layers would keep original components of aeolian dust, whose $\delta^7Li$ value can represent that of the UCC (Sauzéat et al., 2015).

Secondly, the $\delta^7Li_{leachate}$ of S0, L1SS1, L1SS2, L1LL2, and upper S1-1 are lower than $\delta^7Li_{residue}$ (Fig. 2). These layers may have only undergone the processes of weathering and eluviation as the stage I. They were not or only slightly affected by stages II, ...N. During these processes, eluviation solution carries away $^7Li$, leaving $^6Li$ preferentially adsorbed by clay minerals. The low $\delta^7Li_{leachate}$ in these layers indicate weak pedogenic processes, resulting in limited adsorption of $^7Li$ by clays. The limited adsorption of $^7Li$ may be due to rapid infiltration of soil solution along the weakly developed paleosol layers with low clays and coarse particles (Fig. 2). Accompanying the rapid infiltration within porous sediments, $^6Li$ in soil solution may migrate into underlying loess, resulting in lower $\delta^7Li_{leachate}$, such as in the L1LL2.

Furthermore, an increase in $\delta^7Li_{leachate}$ and even higher than $\delta^7Li_{residue}$ would indicate strong pedogenic processes of weathering, eluviation, migration and CCA in the paleosol or weak paleosol layers, such as in the lower parts of the L1SS1 and L1SS2. In particular, there is a gradual increase $\delta^7Li_{leachate}$ from top to bottom of the S1 layer (Fig. 2, red arrows). It exceeds the $\delta^7Li_{residue}$ and reaches the highest $\delta^7Li_{leachate}$ value in the CCA layer at the S1 bottom (Fig. 2, light green shadow). The increasing $\delta^7Li_{leachate}$ suggests more adsorption of $^7Li$ by clays. High $[Li]_{leachate}$ indicates strong leaching as a result of intense weathering, supported by high magnetic susceptibility and low Rb/Sr ratios (Chen et al., 1999). The increasing in clay content from intense weathering as indicated by high CIA would also result in higher degree of $^7Li$ adsorption. The most important mechanism for post-depositional adsorptions of Li in paleosol layers is slow infiltration of soil solution along the paleosol layers with high clay content and fine particles, resulting in long period of interaction between soil solution and clays (Figs. 2 and 4). As a result, $\delta^7Li_{leachate}$ increase gradually and could even exceed the $\delta^7Li_{residue}$ (Fig. 2).

As discussed above, variation in $[Li]_{leachate}$ of loess sediments at various layers provides more detailed information on pedogenic processes of loess-paleosol sequences. The relative uniform $[Li]_{leachate}$ confirms that loess layers have very weak or limited pedogenic processes of weathering and eluviation. On the contrary, the decreased $[Li]_{leachate}$ in upper parts of paleosol layers indicate that decomposition of silicate minerals in paleosol layers releases Li, which rapidly infiltrate downward with soil solution (stage I, Fig. 4a). As weathering and eluviation of upper sediments intensified and became deeply-developed paleosol as the stage II, Li in soil solution migrate into underlying layers and easily adsorbed by the clays, resulting in increasing $\delta^7Li_{leachate}$. It means that the upper section of paleosol layers experienced strongest pedogenesis (Fig. 2). As a result of superimposed pedogenic processes, i.e. stage N ($N \geq 3$), the gradually increased $\delta^7Li_{leachate}$ towards the bottom of the S1 layer suggest slow infiltration of soil solution along the paleosol layers, with constant adsorption by clays. Finally, highest $\delta^7Li_{leachate}$ in the S1 bottom indicates limited weathering, supported by coarser grains, and lowest magnetic susceptibility, Rb/Sr and CIA (Fig. 2).

## 6. CONCLUSIONS

We present $[Li]_{leachate}$ and $\delta^7Li_{leachate}$ data from the Luochuan loess-paleosol sequence since the last interglacial. The $[Li]_{leachate}$ and $\delta^7Li_{leachate}$ variations can be used to trace pedogenic processes of loess-paleosol sediments after deposition. Our main conclusions are as follows:

(1) The $[Li]_{leachate}$ and $\delta^7Li_{leachate}$ from loess and paleosol sediments in Luochuan samples display large variations; $[Li]_{leachate}$ vary from 0.39 to 1.97 μg/g and $\delta^7Li_{leachate}$ from −6.55‰ to +12.88‰.

(2) Li adsorbed by clay minerals (exchangeable Li) is the main source of Li in 1 M HAc acid-leaching fraction of loess-paleosol, since Li from dissolution of both silicate and carbonate minerals accounts for limited proportions of the $[Li]_{leachate}$.
(3) The variations in $[Li]_{leachate}$ and $\delta^7Li_{leachate}$ of loess-paleosol sediments reflect soil migration processes and the magnitude of pedogenic processes in loess-paleosol sequence with different degree of weathering.

## Declaration of Competing Interest

The authors declared that they have no conflicts of interest to this work. We declare that we do not have any commercial or associative interest that represents a conflict of interest in connection with the work submitted.


### ACKNOWLEDGEMENTS

Thanks to Youbin Sun, XinYang Chen, HengCi Tian and Kangjun Huang for constructive discussions and advices that helped improve the initial manuscript. Constructive and detailed comments from Xiao-Ming Liu and two other anonymous reviewers, and efficient editorial handling by Fangzhen Teng and Jeffrey G. Catalano are gratefully acknowledged. This work was supported by the CAS Interdisciplinary Innovation Team and NSFC (41930863).


## APPENDIX A. SUPPLEMENTARY MATERIAL

Supplementary data to this article can be found online at https://doi.org/10.1016/j.gca.2021.02.021.

### REFERENCES


Beck J. W., Zhou W. J., Li C., Wu Z. K., White L., Xian F., Kong X. F. and An Z. S. (2018) A 550,000-year record of East Asian monsoon rainfall from $^{10}$Be in loess. *Science* **360**, 877–881.

Bohlin M. S. and Bickle M. J. (2019) The reactive transport of Li as a monitor of weathering processes in kinetically limited weathering regimes. *Earth Planet. Sci. Lett.* **511**, 233–243.

Chen J., An Z. S. and Head J. (1999) Variation of Rb/Sr ratios in the loess-paleosol sequences of Central China during the last 130,000 years and their implications for monsoon paleoclimatology. *Quat. Res.* **51**, 215–219.

Decarreau A., Vigier N., Pálková H., Petit S., Vieillard P. and Fontaine C. (2012) Partitioning of lithium between smectite and solution: An experimental approach. *Geochim. Cosmochim. Acta* **85**, 314–325.

Feng Z. D. and Wang H. B. (2006) Geographic variations in particle size distribution of the last interglacial pedocomplex S1 across the Chinese Loess Plateau: Their chronological and pedogenic implications. *Catena* **65**, 315–328.

Gallet S., Jahn B. and Torii M. (1996) Geochemical characterization of the Luochuan loess-paleosol sequence, China, and paleoclimatic implications. *Chem. Geol.* **133**, 67–88.

Gou L. F., Jin Z. D., Pogge von Strandmann P. A. E., Li G., Qu Y. X., Xiao J., Deng L. and Galy A. (2019) Li isotopes in the middle Yellow River: Seasonal variability, sources and fractionation. *Geochim. Cosmochim. Acta* **248**, 88–108.

Guo F., Clemens S. C., Wang T., Wang Y., Liu Y. M., Wu F., Liu X. X., Jin Z. D. and Sun Y. B. (2021) Monsoon variations inferred from high-resolution geochemical records of the Linxia loess/paleosol sequence, western Chinese Loess Plateau. *Catena* **198** 105019.

Guo Z. T., Liu D. S. and An Z. S. (1994) Paleosols of the last 0.15 Ma in the Weinan loess section and their paleoclimatic significance. *Quat. Sci.* **14**, 256–269 (in Chinese with English abstract).

He M. Y., Luo C. G., Lu H., Jin Z. D. and Deng L. (2019) Measurements of lithium isotopic compositions in coal using MC-ICP-MS. *J. Anal. At. Spectrom.* **34**, 1773–1778.

Hindshaw R. S., Tosca R., Goût T. L., Farnan I., Tosca N. J. and Tipper E. T. (2019) Experimental constraints on Li isotope fractionation during clay formation. *Geochim. Cosmochim. Acta* **250**, 219–237.

Hofmann A. E., Bourg I. C. and DePaolo D. J. (2012) Ion desolation as a mechanism for kinetic isotope fractionation in aqueous systems. *Proc. Natl. Acad. Sci. USA* **109**, 18689–18694.

Huh Y., Chan L. H. and Chadwick O. (2002) Lithium isotopes as a probe of weathering processes: Hawaiian soil climosequence. *Geochim. Cosmochim. Acta* **66**(15A), A346.

Huang T. Y., Teng F. Z., Rudnick R. L., Chen X. Y., Hu Y., Liu Y. S. and Wu F. Y. (2019) Heterogeneous potassium isotopic composition of the upper continental crust. *Geochim. Cosmochim. Acta* **278**, 122–136.

Jia Y. F., Huang C. C., Pang J. L. and Mao L. J. (2007) Variation of the lithium-barium ratio in the Holocene loess-paleosol profiles in the south of the Chinese Loess Plateau: Implications for pedogenic weathering intensity. *Soil Sci.* **172**, 925–940.

Jin C. S., Liu Q. S., Xu D. K., Sun J. M., Li C. G., Zhang Y., Han P. and Liang W. T. (2019) A new correlation between Chinese loess and deep-sea $\delta^{18}$O records since the middle Pleistocene. *Earth Planet. Sci. Lett.* **506**, 441–454.

Kemp R. A. (2001) Pedogenic modification of loess: Significance for palaeoclimatic reconstructions. *Earth-Sci. Rev.* **54**, 145–156.

Kasemann S. A., Jeffcoate A. B. and Elliott T. (2005) Lithium isotope composition of basalt glass reference material. *Anal. Chem.* **77**, 5251–5257.

Li Y., Song Y. G., Zeng M. X., Lin W. W., Orozbaev R., Cheng L. Q. and Chen X. L. (2018) Evaluating the paleoclimatic significance of clay mineral records from a late Pleistocene loess-paleosol section of the Ili Basin. *Quat. Res.* **89**, 660–673.

Li G. and West A. J. (2014) Evolution of Cenozoic seawater lithium isotopes: Coupling of global denudation regime and shifting seawater sinks. *Earth Planet. Sci. Lett.* **401**, 284–293.

Li W. S. and Liu X.-M. (2020) Experimental investigation of lithium isotope fractionation during kaolinite adsorption: Implications for chemical weathering. *Geochim. Cosmochim. Acta* **284**, 156–172.

Li W. S., Liu X.-M. and Chadwick O. A. (2020) Lithium isotope behavior in Hawaiian regoliths: Soil-atmosphere-biosphere exchanges. *Geochim. Cosmochim. Acta* **285**, 175–192.

Lin J., Liu Y. S., Hu Z. C., Yang L., Chen K., Chen H. B., Zong K. Q. and Gao S. (2016) Accurate determination of lithium isotope ratios by MC-ICP-MS without strict matrix-matching by using a novel washing method. *J. Anal. At. Spectrom.* **31**, 390–397.

Lin J., Liu Y. S., Hu Z. C., Chen W., Zhang L. and Chen H. H. (2019) Accurate measurement of lithium isotopes in eleven carbonate reference materials by MC-ICP-MS with soft extraction mode and $10^{12}$ Ω resistor high-gain faraday amplifiers. *Geostand. Geoanal. Res.* **43**, 277–289.

Liu X.-M. and Rudnick R. L. (2011) Constraints on continental crustal mass loss via chemical weathering using lithium and its isotopes. *Proc. Natl. Acad. Sci. USA* **108**, 20873–20880.

Liu X.-M., Wanner C., Rudnick R. L. and McDonough W. F. (2015) Processes controlling $\delta^7$Li in rivers illuminated by study of streams and groundwaters draining basalts. *Earth Planet. Sci. Lett.* **409**, 212–224.

Ma L., Sun Y. B., Jin Z. D., Bao Z. A., Zhang P., Meng Z. K., Yuan H. L., Long X. P., He M. Y. and Huang K. J. (2019) Tracing changes in monsoonal precipitation using Mg isotopes in Chinese loess deposits. *Geochim. Cosmochim. Acta* **259**, 1–16.

Ma T. T., Weynell M., Li S. L., Liu Y. S., Chetelat B., Zhong J., Xu S. and Liu C. Q. (2020) Lithium isotope compositions of the Yangtze River headwaters: Weathering in high-relief catchments. *Geochim. Cosmochim. Acta* **280**, 46–65.

Millot R. and Girard J. P. (2007) Lithium isotope fractionation during adsorption onto mineral surfaces. *3rd International Meeting of Clays in Natural & Engineered Barriers for Radioactive Waste Confinement*, 307–308.

Misra S. and Froelich P. N. (2012) Lithium isotope history of Cenozoic seawater: Changes in silicate weathering and reverse weathering. *Science* **335**, 818–823.

Nesbitt H. W. and Young G. M. (1982) Early Proterozoic climates and plate motions inferred from major element chemistry of lutites. *Nature* **299**, 715–717.

Penniston-Dorland S., Liu X. M. and Rudnick R. L. (2017) Lithium isotope geochemistry. *Rev. Mineral. Geochem.* **82**, 165–217.

Pistiner J. S. and Henderson G. M. (2003) Lithium-isotope fractionation during continental weathering processes. *Earth Planet. Sci. Lett.* **214**, 327–339.

Pogge von Strandmann P. A. E., Kasemann S. A. and Wimpenny J. B. (2020) Lithium and lithium isotopes in Earth's surface cycles. *Elements* **16**(4), 253–258.

Rosner M., Ball L., Peucker-Ehrenbrink B., Blusztajn J., Bach W. and Erzinger J. (2007) A simplified, accurate and fast method for lithium isotope analysis of rocks and fluids, and $\delta^7$Li values of seawater and rock reference materials. *Geostand. Geoanal. Res.* **31**, 77–88.

Rudnick R. L., Tomascak P. B., Njo H. B. and Gardner L. R. (2004) Extreme lithium isotopic fractionation during continental weathering revealed in saprolites from South Carolina. *Chem. Geol.* **212**, 45–57.

Sauzéat L., Rudnick R. L., Chauvel C., Garçon M. and Tang M. (2015) New perspectives on the Li isotopic composition of the upper continental crust and its weathering signature. *Earth Planet. Sci. Lett.* **428**, 181–192.

Sun Y. B., Wang X. L., Liu Q. S. and Clemens S. C. (2010) Impacts of post-depositional processes on rapid monsoon signals recorded by the last glacial loess deposits of northern China. *Earth Planet. Sci. Lett.* **289**, 171–179.

Sun Y. B., Yin Q. Z., Crucifix M., Araya-Melo P., Liu W. G., Qiang X. K., Liu Q. S., Zhao H., Liang L. J., Chen H. Y., Li Y., Zhang L., Dong G. C., Li M., Zhou W. J., Berger A. and An Z. S. (2019) Diverse manifestations of the mid-Pleistocene climate transition. *Nat. Commun.* **10**, 352.

Taylor H. L., Duivestein K. I. J., Farkas J., Dietzel M. and Dosseto M. (2019) Technical note: Lithium isotopes in dolostone as a palaeo-environmental proxy - an experimental approach. *Clim. Past* **15**, 635–646.

Teng F. Z., McDonough W. F., Rudnick R. L., Dalpe C., Tomascak P. B., Chappell B. W. and Gao S. (2004) Lithium isotopic composition and concentration of the upper continental crust. *Geochim. Cosmochim. Acta.* **68**, 4167–4178.

Teng F. Z., Li W. Y., Rudnick R. L. and Gardner L. R. (2010) Contrasting lithium and magnesium isotope fractionation during continental weathering. *Earth Planet. Sci. Lett.* **300**, 63–71.

Teng F. Z., Watkins J. and Dauphas N. (2017) Non-Traditional Stable Isotopes. *Rev. Mineral. Geochem.* **82**, 885.

Tian S. H., Hou Z. Q., Su A. N., Hou K. J., Hu W. J., Li Z. Z., Zhao Y., Gao Y. G. and Li Y. H. (2012) Separation and precise measurement of lithium isotopes in three reference materials using multi collector-inductively coupled plasma mass spectrometry. *Acta Geol. Sinica* **86**, 1297–1305.

Tomascak P. B., Magna T. S. and Dohmen R. (2016) *Advances in Lithium Isotope Geochemistry*. Springer International Publishing.

Tsai P. H., You C. F., Huang K. F., Chung C. H. and Sun Y. B. (2014) Lithium distribution and isotopic fractionation during chemical weathering and soil formation in a loess profile. *J. Asian Earth Sci.* **87**, 1–10.

Verney-Carron A., Vigier N. and Millot R. (2011) Experimental determination of the role of diffusion on Li isotope fractionation during basaltic glass weathering. *Geochim. Cosmochim. Acta* **75**, 3452–3468.

Vigier N., Decarreau A., Millot R., Carignan J., Petit S. and France-Lanord C. (2008) Quantifying Li isotope fractionation during smectite formation and implications for the Li cycle. *Geochim. Cosmochim. Acta* **72**, 780–792.

Wei H. Z., Lei F., Jiang S. Y., Lu H. Y., Xiao Y. K., Zhang H. Z. and Sun X. F. (2015) Implication of boron isotope geochemistry for the pedogenic environments in loess and paleosol sequences of central China. *Quat. Res.* **83**, 243–255.

Wimpenny J., Colla C. A., Yu P., Yin Q. Z., Rustad J. R. and Casey W. H. (2015) Lithium isotope fractionation during uptake by gibbsite. *Geochim. Cosmochim. Acta* **168**, 133–150.

Wu N. Q., Li F. J. and Rousseau D. D. (2018) Terrestrial mollusk records from Chinese loess sequences and changes in the East Asian monsoonal environment. *J. Asian Earth Sci.* **155**, 35–48.

Yang J. D., Chen J., Tao X. C., Li C. L., Ji J. F. and Chen Y. (2001) Sr isotope ratios of the acid-leached loess residues from Luochuan, China: A tracer of continental weathering intensity over the past 2.5 Ma. *Geochem. J.* **35**, 403–412.

*Associate editor:* Fang-Zhen Teng